Performance Analysis of Volume-Based Spectrum Sensing for Cognitive Radio

Lei Huang, *Member, IEEE*, Cheng Qian, *Student Member, IEEE*, Yuhang Xiao, and Q. T. Zhang, *Fellow, IEEE*

***Abstract*—In this work, the volume-based method for spectrum sensing is analyzed, which is able to provide the desirable properties of constant false-alarm rate, robustness against deviation from independent and identically distributed (IID) noise and being free of noise uncertainty. By computing the first and second moments for the signal-absence and signal-presence hypotheses together with using the Gamma distribution approximation, we derive accurate analytic formulae for the false-alarm and detection probabilities for IID noise situations. This enables us to develop theoretical decision threshold as well as receiver operating characteristic. Numerical results are presented to validate our theoretical findings.**

***Index Terms*—Cognitive radio, spectrum sensing, volume, Gamma distribution, multiple antenna.**

I. Introduction

As a fundamental element in cognitive radio (CR) [1], [2], spectrum sensing has received much attention in the literature. Basically, a secondary (unlicensed) user (SU) is allowed to borrow the frequency channels from the primary (licensed) users (PUs) in the same CR network provided that it does not cause intolerable interference to the latter. To maximize the spectral utilization and minimize the harmful interference to the PUs, the SU usually needs to employ multiple antennas to reliably detect the PUs particularly at low signal-to-noise ratio (SNR) and/or small samples [3], [4]. Nevertheless, the multi-antenna receiver is typically uncalibrated or contains calibration error in practice, thereby calling for robust methodologies for spectrum sensing.

Numerous methodologies have been devised for spectrum sensing in the literature, varying from non-blind approach to blind approach. Basically, the non-blind algorithms need to employ some *a priori* knowledge of the noise, signal or channel to construct their test statistics, such as the energy detection (ED) method [5]–[7] and feature detection approaches [8]–[11]. With the known noise variance, it is proved that the ED method is optimal for independent and identically distributed (IID) observations. Nevertheless, its optimality cannot be guaranteed for the situation of unknown noise variance because it is rather sensitive to the noise uncertainty in the estimated noise variance, particularly for the non-IID noise. It is shown in [10], [11] that the feature detector is robust against the noise uncertainty and provide superior detection performance. However, it usually suffers from synchronization errors and frequency offsets in practical situations, thereby limiting its applications. Indeed, the presence of primary signals not only changes the energy in the observation data but the correlation structure as well. The correlation structure inherent in the observation covariance matrix leads to the most spread-out eigenspectrum, providing a good indication for the primary signals. In addition, unlike the ED and feature detection schemes, the eigenvalue-based approach is free of the noise variance and signal features, thereby being a blind detector. As a result, the eigenvalue-based spectrum sensing approaches have received much attention [3], [12]–[16]. As a generalized likelihood ratio test (GLRT) variant, the spherical test (ST) detector [17] is able to reliably identify the correlated signals embedded in additive IID noise. In fact, the ST detector is equivalent to the eigenvalue arithmetic-to-geometric mean (AGM) algorithm [18]. Nevertheless, it is indicated in [19] that, as the locally most powerful invariant test for sphericity, John's detector [20] is superior to the ST detector when the numbers of antennas and samples tend to infinity at the same rate. As a matter of fact, the spectrum sensing algorithms above are developed upon the IID noise assumption and thereby not robust against the deviation from the IID noise, which is quite relevant in the real-world applications since the SU receiver is typically uncalibrated. Even though the receiver can be calibrated, the calibration error makes the thermal noise to be non-ideal IID to some extent, which poses a big challenge for practical spectrum sensing. Indeed, besides the non-IID noise, the radio frequency (RF) IQ imbalance [21], [22] can also lead to performance degradation for the spectrum sensing methods, which, however, is beyond the scope of this paper.

Some approaches have been suggested for robust spectrum sensing in the literature, such as the GLRT test [23], independence test [24], Hadamard ratio test [25], [26], Gerschgorin disk test [27], locally most powerful invariant test (LMPIT) [28] and volume-based test approaches [29]. Being robust against the non-IID noise and derived in the GLRT paradigm, the Hadamard ratio approach [30]–[32] has received much attention in the community of spectrum sensing, such as [25], [26]. In this approach, spectrum sensing is cast as the issue of

Manuscript received March 4, 2014; revised June 6, 2014; accepted July 29, 2014. Date of publication August 7, 2014; date of current version January 7, 2015. The work described in this paper was supported by the National Natural Science Foundation of China (No. 61222106) and by the Shenzhen Kongqie talent program under Grant KQC201109020061A. The associate editor coordinating the review of this paper and approving it for publication was G. V. V. Sharma.

L. Huang, C. Qian, and Y. Xiao are with Department of Electronic and Information Engineering, Harbin Institute of Technology Shenzhen Graduate School, Shenzhen 518055, China (e-mail: dr.lei.huang@ieee.org).

Q. T. Zhang is an Emeritus Professor with Department of Electronic Engineering, City University of Hong Kong, Kowloon, Hong Kong (e-mail: qtzhang@ieee.org).

Color versions of one or more of the figures in this paper are available online at http://ieeexplore.ieee.org.

Digital Object Identifier 10.1109/TWC.2014.2345660

distinguishing between a diagonal matrix and an arbitrary Hermitian matrix. A variant of the Hadamard ratio approach for spectrum sensing has been proposed in [25], where the number of PUs needs to be known *a priori* to the receiver, which, however, is not rational in the practical spectrum sensing situations. On the other hand, the performance of the Hadamard ratio algorithm for spectrum sensing has been analyzed in [23], [24]. However, as pointed out in [29], although the Hadamard ratio test is robust against the non-IID noise, its detection performance needs to be further enhanced. Unlike the Hadamard ratio approach, the volume-based detector [29] is able to employ the correlation among the primary signals to further increase the denominator of the test statistic, leading to significant reduction in the test variable under the signal-presence hypothesis. This eventually leads to considerable improvement in detection performance for the volume-based approach.

It is worth pointing out that the volume-based detector is originally developed in [29] for real-valued observation and its detection performance has not yet been analyzed, which is the major contribution of this work. In particular, by computing the first and second moments for the signal-absence and signal-presence hypotheses together with using the Gamma distribution approximation, we derive accurate analytic formulae for the false-alarm and detection probabilities for the scenario of IID noise. This enables us to develop the theoretical decision threshold for practical primary signal detection as well as receiver operating characteristic (ROC) for performance evaluation.

The remainder of the paper is organized as follows. Section II presents the problem formulation, including the signal model as well as relevant sensing solution. Performance analysis of the volume-based method is provided in Section III. Simulation results are presented in Section IV. Finally, conclusions are drawn in Section V.

Throughout this paper, we use boldface uppercase letter to denote matrix, boldface lowercase letter for column vector, and lowercase letter for scalar quantity. Superscripts $(\cdot)^{\mathrm{T}}$ and $(\cdot)^{\mathrm{H}}$ represent transpose and conjugate transpose, respectively. The $E[a]$ and $\hat{a}$ denote the expected value and estimate of a, respectively. The $|\boldsymbol{A}|$ is the determinant of $\boldsymbol{A}$, $\mathrm{diag}(\cdot)$ stands for a diagonal matrix and $\boldsymbol{I}_M$ represents the $M \times M$ identity matrix. The $\boldsymbol{x} \sim \mathcal{N}(\boldsymbol{\mu}, \boldsymbol{\Sigma})$ means $\boldsymbol{x}$ follows a complex Gaussian distribution with mean $\boldsymbol{\mu}$ and covariance matrix $\boldsymbol{\Sigma}$, and $\sim$ signifies "distributed as." The $\mathbf{R} \sim \mathcal{W}_M(N, \boldsymbol{\Sigma})$ denotes a complex Wishart distribution with N degrees of freedom and associated covariance matrix $\boldsymbol{\Sigma}$. The a_{ij} stands for the (i, j) element of $\boldsymbol{A}$ and $\boldsymbol{A} \succ \boldsymbol{B}$ means that $\boldsymbol{A} - \boldsymbol{B}$ is a positive definite matrix.

II. Problem Formulation

A. Signal Model

Consider the standard signal model where a SU with M antennas tries to detect the signals emitted by d PUs with single antenna:

$$\boldsymbol{x}_t = \boldsymbol{H}\boldsymbol{s}_t + \boldsymbol{n}_t. \tag{1}$$

Here, $\boldsymbol{H} \in \mathbb{C}^{M \times d}$ denotes the channel matrix between the PUs and SU, which is unknown deterministic during the sensing period, and the

$$\boldsymbol{x}_t = [x_1(t), \ldots, x_M(t)]^{\mathrm{T}} \tag{2}$$

$$\boldsymbol{s}_t = [s_1(t), \ldots, s_d(t)]^{\mathrm{T}} \tag{3}$$

$$\boldsymbol{n}_t = [n_1(t), \ldots, n_M(t)]^{\mathrm{T}} \tag{4}$$

are the observation, signal and noise vectors, respectively. Suppose that $s_i(t) \sim \mathcal{N}(0, \sigma_{s_i}^2)(i = 1, \ldots, d)$ with $\sigma_{s_i}^2$ being the ith unknown signal variance, and that $n_i(t) \sim \mathcal{N}(0, \tau_i)(i = 1, \ldots, M)$ with τ_i being the unknown noise variance. Note that τ_i is not necessarily equal to τ_j for $i \neq j$ in practice, which corresponds to the case of uncalibrated receiver. Furthermore, we assume that the noises are statistically independent of each other and also independent of the signals. In the signal-absence hypothesis $\mathcal{H}_0$, the population covariance matrix of the observation $\boldsymbol{x}_t$ is $\boldsymbol{\Sigma} = E[\boldsymbol{x}_t \boldsymbol{x}_t^{\mathrm{H}}] = \mathrm{diag}(\tau_1, \ldots, \tau_M)$. However, the presence of primary signals destroys this diagonal structure, leading to

$$\boldsymbol{\Sigma} = \boldsymbol{H}\boldsymbol{\Sigma}_s\boldsymbol{H}^{\mathrm{H}} + \mathrm{diag}(\tau_1, \ldots, \tau_M) \tag{5}$$

where $\boldsymbol{\Sigma}_s = E[\boldsymbol{s}_t \boldsymbol{s}_t^{\mathrm{H}}]$. Therefore, the spectrum sensing issue is cast as the binary hypothesis test:

$$\mathcal{H}_0 : \boldsymbol{\Sigma} = \mathrm{diag}(\tau_1, \ldots, \tau_M) \tag{6}$$

$$\mathcal{H}_1 : \boldsymbol{\Sigma} \succ \mathrm{diag}(\tau_1, \ldots, \tau_M) \tag{7}$$

where $\mathcal{H}_1$ denotes the signal-presence hypothesis. The problem at hand is to test $\boldsymbol{\Sigma} = \mathrm{diag}(\tau_1, \ldots, \tau_M)$ for a null hypothesis against all any other possible alternatives of $\boldsymbol{\Sigma}$ by using the noisy observations $\boldsymbol{X} = [\boldsymbol{x}_1, \ldots, \boldsymbol{x}_N]$. Here, N denotes the number of samples which, without loss of generality, is assumed to be not less than the number of antennas, i.e., $N \geq M$.

B. Sensing Solution

The determinant of $\boldsymbol{\Sigma}$ is the hyper-volume of the geometry determined by the row vectors of $\boldsymbol{\Sigma}$. For example, consider the situation of three receiving antennas where the observed data with zero mean and unity variance can be independent, correlated or coherent. The corresponding covariance matrices turn out to be the 3×3 identity matrix, full-rank non-identity matrix and rank-one arbitrary matrix. Fig. 1 plots these geometries, namely, cube, parallelepiped and line, formed by the row vectors of the matrices. We assume that all edges of the geometries are unity such that $\|\boldsymbol{\Sigma}(i,:)\| = 1$ where $\boldsymbol{\Sigma}(i,:)$ is the i-th row of $\boldsymbol{\Sigma}$ and $\|\cdot\|$ is the Euclidean norm. Moreover, the volumes of the cube, parallelepiped and line, are denoted by v_1, v_2 and v_3, respectively. The cube is referring to the situation of signal-absence while the other two geometries correspond to the scenario of signal-presence. For the situation of signal absence, the covariance matrix is a 3×3 identity matrix, meaning that $v_1 = 1$. For the scenario of signal presence, nevertheless, the structure of diagonal matrix is destroyed, resulting in significant volume reduction. Therefore, the volume is able

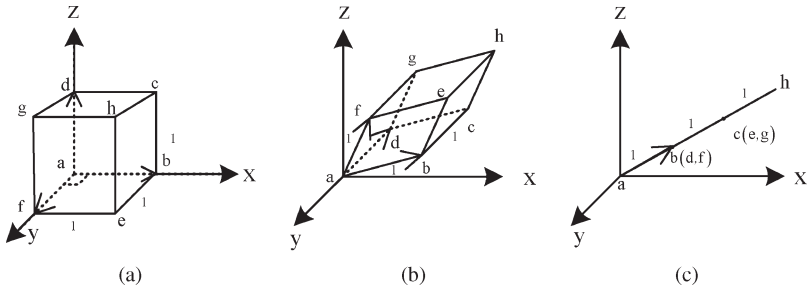

Fig. 1. Volume comparison for uncorrelated, correlated and coherent observations. (a) $v_1 = 1$; (b) $v_2 < v_1$; (c) $v_1 = 0$.

to differentiate the primary signals from the background noise, providing a new approach for accurate spectrum sensing.

In the signal-absence situation, the elements of $\boldsymbol{x}(k)$, i.e., $x_i(t),\ t = 1, \ldots, N,\ i = 1, \ldots, M$, are statistically independent. To utilize the correlation structure for practical spectrum sensing, we need to calculate the sample covariance matrix (SCM) rather than the population covariance matrix $\boldsymbol{\Sigma}$, which is given as

$$\boldsymbol{S} = \frac{1}{N}\sum_{t=1}^{N} \boldsymbol{x}_t \boldsymbol{x}_t^{\mathrm{T}}. \tag{8}$$

Moreover, the edge lengths of the row vectors of the SCM are computed as $\rho_i = \|\boldsymbol{S}(i,:)\| (i = 1, \ldots, M)$. Setting $\boldsymbol{D} = \mathrm{diag}(\rho_1, \ldots, \rho_M)$, the volume of the geometry with unity edge is $|\boldsymbol{D}^{-(1/2)}\boldsymbol{S}\boldsymbol{D}^{-(1/2)}|$. Consequently, we have

$$\xi_{\mathrm{VOL}} \triangleq \frac{|\boldsymbol{S}|}{|\boldsymbol{D}|}. \tag{9}$$

For the scenario of signal-absence, $\boldsymbol{D}^{-(1/2)}\boldsymbol{S}\boldsymbol{D}^{-(1/2)}$ asymptotically approaches the identity matrix as the number of samples tends to infinity, leading to the volume of one. For the situation of signal-presence, however, the correlation structure leads to notable reduction in $|\boldsymbol{S}|$ but considerable increase in $|\boldsymbol{D}|$, eventually leading to significant reduction of the total volume and thereby providing a good indication for the primary signals. Therefore, compared with a predetermined threshold γ_{VOL}, the statistic is able to yield the detection of the PUs. That is

$$\xi_{\mathrm{VOL}} \underset{\mathcal{H}_1}{\overset{\mathcal{H}_0}{\gtrless}} \gamma_{\mathrm{VOL}}. \tag{10}$$

It is worth pointing out that the volume-based detector offers the same expression as the Hadamard ratio test but with a different diagonal matrix in the denominator. The Hadamard ratio rule is given as

$$\xi_{\mathrm{HDM}} \triangleq \frac{|\boldsymbol{S}|}{|\boldsymbol{G}|} \underset{\mathcal{H}_1}{\overset{\mathcal{H}_0}{\gtrless}} \gamma_{\mathrm{HDM}} \tag{11}$$

where $\boldsymbol{G} = \mathrm{diag}(r_{11}, \ldots, r_{MM})$ with $r_{ii} (i = 1, \ldots, M)$ being the main diagonal elements of $\boldsymbol{S}$. Noting that $\boldsymbol{D}^{-(1/2)}\boldsymbol{S}\boldsymbol{D}^{-(1/2)}$ and $\boldsymbol{G}^{-(1/2)}\boldsymbol{S}\boldsymbol{G}^{-(1/2)}$ asymptotically are an identity matrix under $\mathcal{H}_0$, the decision threshold γ_{VOL} is approximately equal to γ_{HDM}. On the other hand, ρ_i is much larger than r_{ii} due to the correlation structure, making

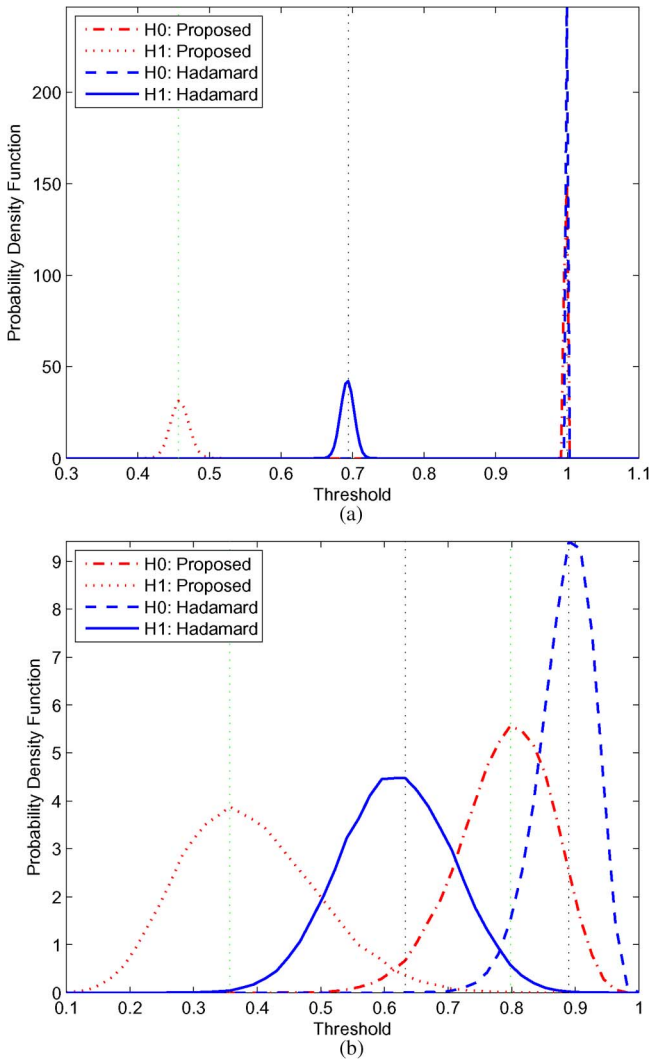

Fig. 2. PDF versus threshold. $M = 4$, $d = 3$ and SNR $= [-2, -3, -4]$ dB. (a) $N = 5000$. (b) $N = 50$.

ξ_{VOL} to be much smaller than ξ_{HDM} under $\mathcal{H}_1$. Therefore, the volume-based approach is able to employ the correlation structure to further enhance the detection performance.

To illustrate the different behaviors of the volume-based and Hadamard ratio approaches, the empirical probability density functions (PDFs) of the test statistics for these two methods are plotted in Fig. 2, where the number of antennas is 4, three primary signals with powers of $[-2, -3, -4]$ dB are assumed to exist in the sensed channel and the noise is IID with unity power. In Fig. 2(a), the number of samples is sufficiently large, i.e., $N = 5000$, so that the SCM is the very accurate estimate

of the population covariance matrix. For the signal-absence situation, the covariance matrix is an identity matrix, which in turn means that the PDF of ξ_{VOL} is equal to that of ξ_{HDM}, as validated in Fig. 2(a). Moreover, it is seen that the PDF under $\mathcal{H}_1$, denoted as p_1, is much farther away from the PDF under $\mathcal{H}_0$, denoted as p_0, of the volume-based detector than that of the Hadamard ratio scheme. Indeed, the Kullback-Leibler (KL) distance between p_0 and p_1 is calculated as $D(p_1\|p_0) = \sum_{i=1}^{Q} p_1(i)\log(p_1(i)/p_0(i))$ with $Q = 200$, which is $D_{\mathrm{VOL}} = 7.8659$ for the volume-based algorithm and $D_{\mathrm{HDM}} = 4.3039$ for the Hadamard ratio approach. The larger KL distance results in considerable enhancement in detection performance for the volume-based algorithm. When the number of samples becomes small, say, $N = 50$, the SCM is the inaccurate estimate of the population one. The corresponding numerical results are depicted in Fig. 2(b). Accordingly, the KL distance of the volume-based approach is $D_{\mathrm{VOL}} = 84.0485$ whereas the KL distance of the Hadamard ratio method is $D_{\mathrm{HDM}} = 59.0912$. Here, we set $Q = 50$. It is seen that the volume-based approach is still superior to the Hadamard ratio testing because it provides a larger KL distance than the latter. This thereby implies that the volume-based algorithm is able to correctly detect the PUs with higher probability than the Hadamard ratio approach especially in small sample and low SNR situations.

To easy the theoretical analysis, the volume-based test statistic is modified as

$$\xi \overset{\Delta}{=} -\log\frac{|\boldsymbol{S}|}{|\boldsymbol{D}|} \underset{\mathcal{H}_1}{\overset{\mathcal{H}_0}{\gtrless}} \gamma. \tag{12}$$

where γ is the decision threshold of the volume-based detector. Note that the volume-based test statistic in (12) has been derived in [29] for accurate and robust spectrum sensing. Nevertheless, its theoretical performance analysis has not yet been investigated. In the next section, exploiting the Gamma distribution approximation, accurate analytic formulae are derived for the false-alarm probability, detection probability, theoretical decision threshold as well as ROC. This enables us to accurately determine the theoretical decision threshold for practical spectrum sensing. Moreover, the analytic expression for the probability of detection can be employed to evaluate the detection performance of the volume-based approach.

III. Performance Analysis

In this section, analytic formulae for the false-alarm probability, detection probability, decision threshold as well as ROC are derived by assuming the additive noise is IID. Note that $|\boldsymbol{S}|/|\boldsymbol{D}| \in [0,1]$ while $-\log(|\boldsymbol{S}|/|\boldsymbol{D}|) \in [0,\infty)$. Therefore, we employ the Gamma approximation with the same support by means of moment matching to determine the distributions of ξ_{VOL} under $\mathcal{H}_0$ and $\mathcal{H}_1$. Since the computation of the first two moments under the signal-absence hypothesis is the simplified case of that under the signal-presence hypothesis, we will first address the detection probability of the volumed-based method.

A. Detection Probability

Let $p_1(y)$ be the PDF of the statistic variable ξ under $\mathcal{H}_1$, which is determined by the following proposition.

Proposition 1: For any antenna number M and sample number N with $N \geq M$, the two-first-moment Gamma approximation to the PDF of ξ under $\mathcal{H}_1$ is

$$p_1(y) \approx \frac{y^{\alpha_1-1}\beta_1^{-\alpha_1}e^{-\frac{y}{\beta_1}}}{\Gamma(\alpha_1)},\ y \in [0,\infty) \tag{13}$$

where $\Gamma(\cdot)$ is the complete Gamma function and

$$\alpha_1 = \frac{\mu_1^2}{\nu_1^2} \tag{14a}$$

$$\beta_1 = \frac{\nu_1^2}{\mu_1} \tag{14b}$$

with μ_1 and ν_1 being the second-order approximation to the mean of ξ and the first-order approximations to the variance of ξ, whose computations are provided in (A.4).

Proof: The proof is seen in Appendix A. ■

It follows from Proposition 1 that the detection probability is computed as

$$P_{\mathrm{d}}(\gamma) \overset{\Delta}{=} \mathrm{Prob}(\xi < \gamma|\mathcal{H}_1) = F(\gamma;\alpha_1,\beta_1) \tag{15}$$

provided that the population covariance matrix $\boldsymbol{\Sigma}$ is given. Here, $F(\gamma;\alpha_1,\beta_1)$ is the cumulative distribution function (CDF) of Gamma distribution. From the constant false-alarm rate (CFAR) perspective, the decision threshold γ usually is determined under the signal-absence hypothesis, which must be deterministic and independent of the noise variance.

B. False Alarm Probability

The false-alarm probability can be easily determined by the following proposition.

Proposition 2: For any antenna number M and sample number N with $N \geq M$, the two-first-moment Gamma approximation to the PDF of ξ under $\mathcal{H}_0$ is

$$p_0(y) \approx \frac{y^{\alpha_0-1}\beta_0^{-\alpha_0}e^{-\frac{y}{\beta_0}}}{\Gamma(\alpha_0)},\ y \in [0,\infty) \tag{16}$$

where

$$\alpha_0 = \frac{\mu_0^2}{\nu_0^2} \tag{17a}$$

$$\beta_0 = \frac{\nu_0^2}{\mu_0} \tag{17b}$$

with μ_0 and ν_0 being the second order approximation to the mean of ξ and the first order approximations to the variance of ξ, whose calculation are given in (B.1).

Proof: The proof is seen in Appendix B. ■

It follows from Proposition 2 that the false-alarm probability is determined as

$$P_{\mathrm{fa}}(\gamma) \overset{\Delta}{=} \mathrm{Prob}(\xi < \gamma|\mathcal{H}_0) = F(\gamma;\alpha_0,\beta_0). \tag{18}$$

Inversely, given a false-alarm probability P_{fa}, the decision threshold can be obtained by numerically inverting

$F(\gamma;\alpha_0,\beta_0)$. That is,

$$\gamma = F^{-1}(P_{\rm fa};\alpha_0,\beta_0) \tag{19}$$

where $F^{-1}(\cdot)$ represents the inverse function of $F(\cdot)$. On the other hand, with the so-obtained threshold, the corresponding detection probability is computed by (15). The mapping between the false-alarm probability and detection probability yields the ROC. Hence, the analytic ROC formula for the volume-based test is

$$P_{\rm d} = F\left[F^{-1}(P_{\rm fa};\alpha_0,\beta_0);\alpha_1,\beta_1\right]. \tag{20}$$

Remark: Note that the IID noise assumption is not required for the volume-based detector but necessary for theoretically deriving the decision threshold, which under the non-IID noise scenario can alternatively be determined by the Monte-Carlo simulation. Nevertheless, it is quite hard to calculate the theoretical threshold of the volume-based approach for non-IID noise, which will be studied in our future work. On the other hand, recall that the volume-based method involves the computations of SCM and determinant, requiring about $\mathcal{O}(M^2N + M^3)$ flops. Some computationally simpler schemes, such as [33]–[36], might be adopted to alleviate the computational intensity of the volume-based approach, which will be our future work.

IV. Numerical Results

Simulation results are presented in this section to validate our derived analytic false-alarm and detection probabilities. Moreover, the superiority of the volume-based approach over the representative approaches for spectrum sensing under the IID and non-IID noise conditions are demonstrated.

A. Analytic False Alarm and Detection Probabilities

In this subsection, the accuracy of the analytic formulae for the false-alarm and detection probabilities is numerically evaluated. For the purpose of comparison, the exact false-alarm and detection probabilities, which are empirically determined by 10^5 Monte Carlo simulation trials, are presented as well. Fig. 3(a) plots the false-alarm probability versus decision threshold in the presence of IID noise, where the number of antennas is $M = 4$ whereas the number of samples is set as $N = [100, 200, 400]$. It is indicated in Fig. 3(a) that the proposed Gamma approximate false-alarm probability is very accurate in terms of fitting the empirical false-alarm probability for IID noise. The simulation results for the derived Gamma approximate and empirical false-alarm probabilities are depicted in Fig. 3(b) for $M = 6$ and $N = [200, 400, 600]$. It is observed that the Gamma approximate $P_{\rm fa}$ is very close to the exact one. This in turn implies that the derived false-alarm probability provides accurate theoretical threshold calculation for practical spectrum sensing.

Now let us examine the accuracy of the detection probability for the proposed Gamma approximation. Similarly, the exact detection probability empirically determined by 10^5 Monte-Carlo simulations are also presented for comparison. In the presence of primary signals, the Rayleigh-fading channel is adopted to evaluate the accuracy of the derived Gamma approximate $P_{\rm d}$, which has been well studied in [37]–[40]. It is shown in [38] that, in the Rayleigh-fading situation, the columns of the channel matrix $\boldsymbol{H}$ follow a complex Gaussian distribution with mean zero and covariance matrix $\boldsymbol{\Psi}$ due to the correlation among the signals at the receiving antennas which cannot be sufficiently spaced for physical size constraints. As is indicated in [37], [38], [40], the correlated Rayleigh-fading channel model is able to precisely characterize the behavior of the practical channels. The (k,ℓ) entry of $\boldsymbol{\Psi}$ is determined as [38, Eq.(27)]

$$\phi_{k\ell} = \frac{\mathcal{I}_0\left(\sqrt{\kappa^2 - 4\pi^2 d_{k\ell}^2 + j4\pi\kappa\sin(\psi)d_{k\ell}}\right)}{\mathcal{I}_0(\kappa)}, \quad (k,\ell = 1,\ldots,M) \tag{21}$$

where $\mathcal{I}_0(\cdot)$ denotes the zero-order modified Bessel function, κ controls the width of the angles-of-arrival (AOAs) of the primary signals impinging upon the receiving antennas of the

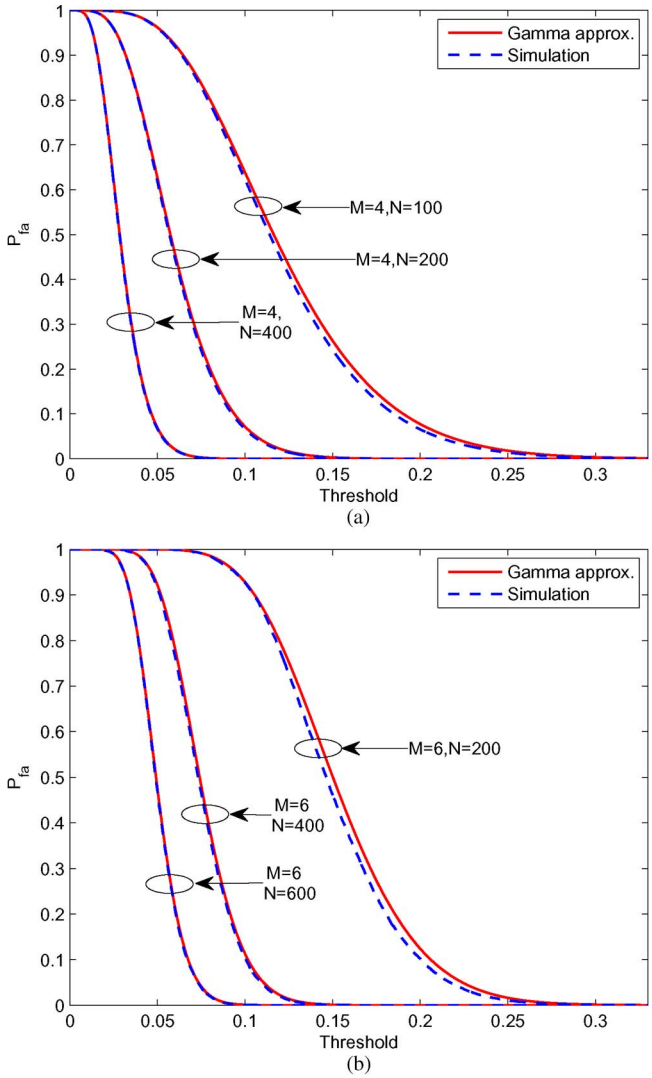

Fig. 3. False alarm probability versus threshold in IID noise. (a) $M = 4$ and N varies from 100, 200 to 400. (b) $M = 6$ and N varies from 200, 400 to 600.

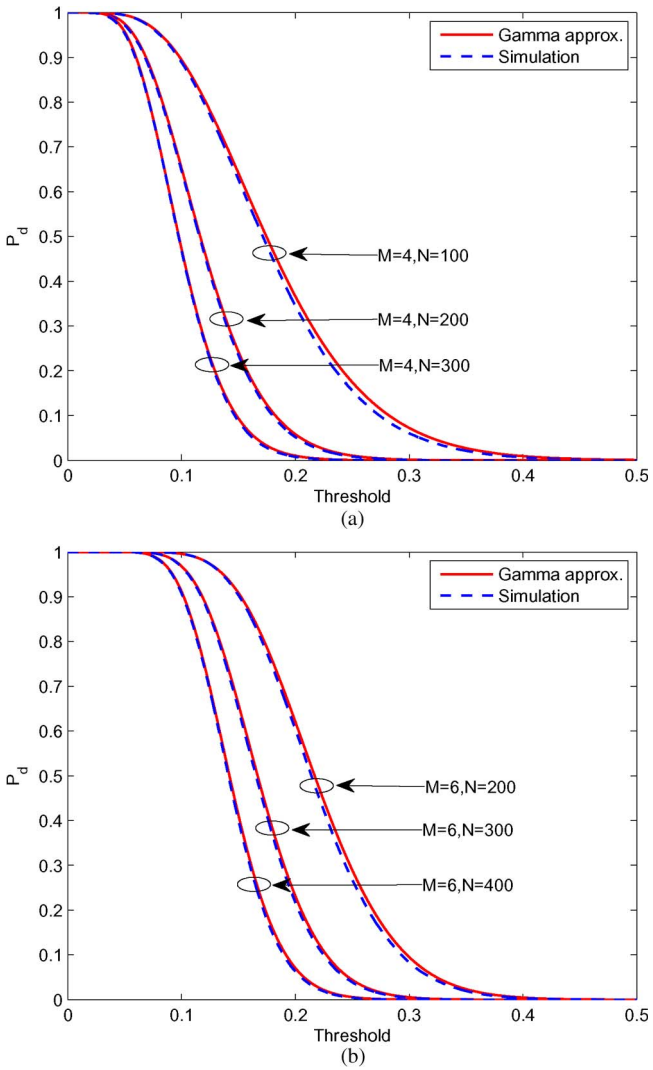

Fig. 4. Detection probability versus threshold for three primary signals in IID noise. $\sigma^2_{s_1} = -5$ dB. (a) $M = 4$ and N varies from 100, 200 to 300. (b) $M = 6$ and N varies from 200, 300 to 400.

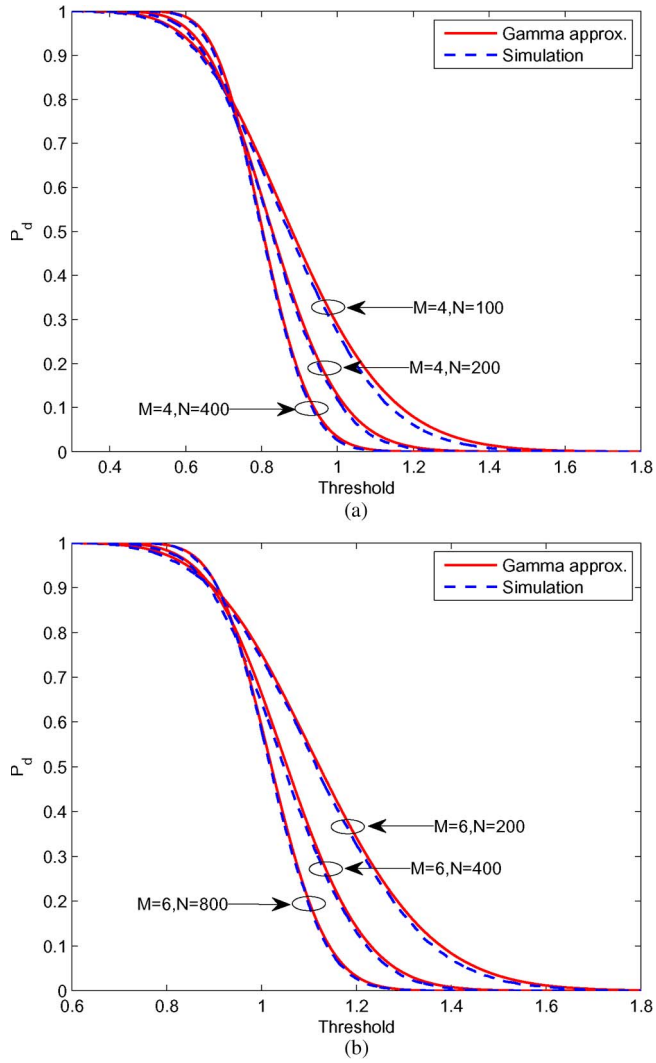

Fig. 5. Detection probability versus threshold for three primary signals in IID noise. $[\sigma^2_{s_1}, \sigma^2_{s_2}, \sigma^2_{s_3}] = [-2, -3, -4]$ dB. (a) $M = 4$ and N varies from 100, 200 to 400. (b) $M = 6$ and N varies from 200, 400 to 800.

SU, which can vary from 0 (isotropic scattering) up to ∞ (extremely non-isotropic scattering), $\psi \in [-\pi, \pi)$ represents the mean direction of the AOAs, and $d_{k\ell}$ stands for the distance, which is normalized with respect to the wavelength λ, between the k-th and ℓ-th antennas of the SU. In the simulation, we set $\kappa = 80$ and $\psi = \pi/2$, and suppose that the antennas of the SU are of the linear uniform array structure with the inter-element distance being $\lambda/2$. As a result, the normalized distance between the adjacent antennas equals 0.5. Without loss of generality, the channel is normalized as $\boldsymbol{g}_i = \boldsymbol{h}_i/\|\boldsymbol{h}_i\|$ and the noise variance is set to one for IID noise.

Fig. 4(a) demonstrates the numerical results for a single primary signal in the Rayleigh fading channel and under the situation of IID noise. Here, the number of antennas is 4, the number of samples increases from 100, 200 to 300, and the power of the primary signal is set as -5 dB. It is implied that the derived detection probability is able to accurately predict the detection performance for the volume-based approach. Fig. 4(b) plots the Gamma approximate and exact detection probability of the volume-based detection method for IID noise, where the number of antennas is 6, the number of samples increases from 200, 300 to 400, and the signal power is the same as that in Fig. 4(a). The numerical results again validate the efficiency of the derived Gamma approximate P_{d}. The numerical results for three primary signals with powers of $[-2, -3, -4]$ dB are plotted in Fig. 5. The number of antennas is 4 and the number of samples is set as [100, 200, 400] in Fig. 5(a). We can observe that the proposed Gamma approximate detection probability is quite precise in terms of fitting the exact one. In Fig. 5(b), the number of antennas and number of samples are set as $M = 6$ and $N = [200, 400, 800]$, respectively. It is observed that the derived P_{d} is very accurate in terms of predicting the detection performance for the volume-based algorithm.

B. Detection Performance

In this subsection, let us evaluate the robustness as well as accuracy of the volume-based detection algorithm for complex-valued observed data by comparing its empirical ROC with those of other representative methods. In particular, the decision

threshold is varied to calculate the false-alarm probability and its corresponding detection probability, leading to the ROC curve. For the purpose of comparison, the numerical results of the John's, AGM (or ST), Hadamard ratio as well as ED detectors are provided. Recalling that the true noise variance is unknown *a priori* to the receiver in practice, the ED approach is thereby used herein as the benchmark. In addition, the Rayleigh fading channel model addressed above is employed. All the numerical results are obtained from 10^5 Monte Carlo trials.

The ROCs of the volume-based, AGM, John's, Hadamard ratio and ED algorithms in Rayleigh fading channel and IID noise are demonstrated in Fig. 6, where the number of antennas equals 4. It is indicated from Fig. 6(a), where the number of samples is 10, the number of primary signals is one and its power equals 8 dB, that the volume-based approach is superior to the AGM and Hadamard ratio methods but inferior to John's detector which is known to be the locally most powerful invariant test for sphericity. Moreover, all of them are inferior to the true noise variance based ED approach. The similar results are observed in Fig. 6(b), where the numbers of antennas and samples remain unchanged while the number of primary signals increases to three and their powers are set as $[\sigma_{s_1}^2, \sigma_{s_2}^2, \sigma_{s_3}^2] = [5, 2, 0]$ dB. This indicates that the volume-based detector surpasses the AGM and Hadamard ratio methods but is not as accurate as John's approach in the scenario of IID noise. However, as the sample number increases to 50, the volume-based algorithm is able to provide the same accuracy as John's algorithm which has been proved to be the most powerful for the small sample case. The numerical results for the same signal parameters and channel model but different noise model, namely, the non-IID noise, are plotted in Fig. 7, where the noise variances are $[1, 1.7, -0.7, -2]$ dB and the averaged noise variance is equal to one. Under such a non-IID noise condition, the volume-based detector is capable of offering the best detection performance among the blind methods. This in turn implies that the volume-based approach is superior to the Hadamard ratio method in accuracy and to the AGM and John's schemes in robustness against the deviation of IID noise. As pointed out in Section II-B, the Hadamard ratio algorithm cannot utilize the correlation among the primary signals to improve the detection accuracy although it is robust against the non-IID noise. Unlike the Hadamard ratio approach, the denominator in the volume-based test expression considerably increases while the numerator, i.e., the determinant of covariance matrix, significantly decreases due to the signal correlation, finally resulting in notable reduction in the total volume. This is why the volume-based test scheme is able to provide the superiority over the Hadamard ratio method. As the AGM and John's detectors are derived from the assumption of IID noise, they cannot provide the robustness against the non-IID noise.

The ROCs of various algorithms for $M = 6$ and IID noise are depicted in Fig. 8. Similar to the numerical results in Fig. 6, the volume-based method is superior to the AGM and Hadamard ratio schemes but inferior to John's scheme in detection performance. The numerical results of various methods for $M = 6$ and non-IID noise are shown in Fig. 9, where the noise powers are set as $[-1.2, -0.3, 2.6, -0.8, 2.4, -2.7]$ dB.

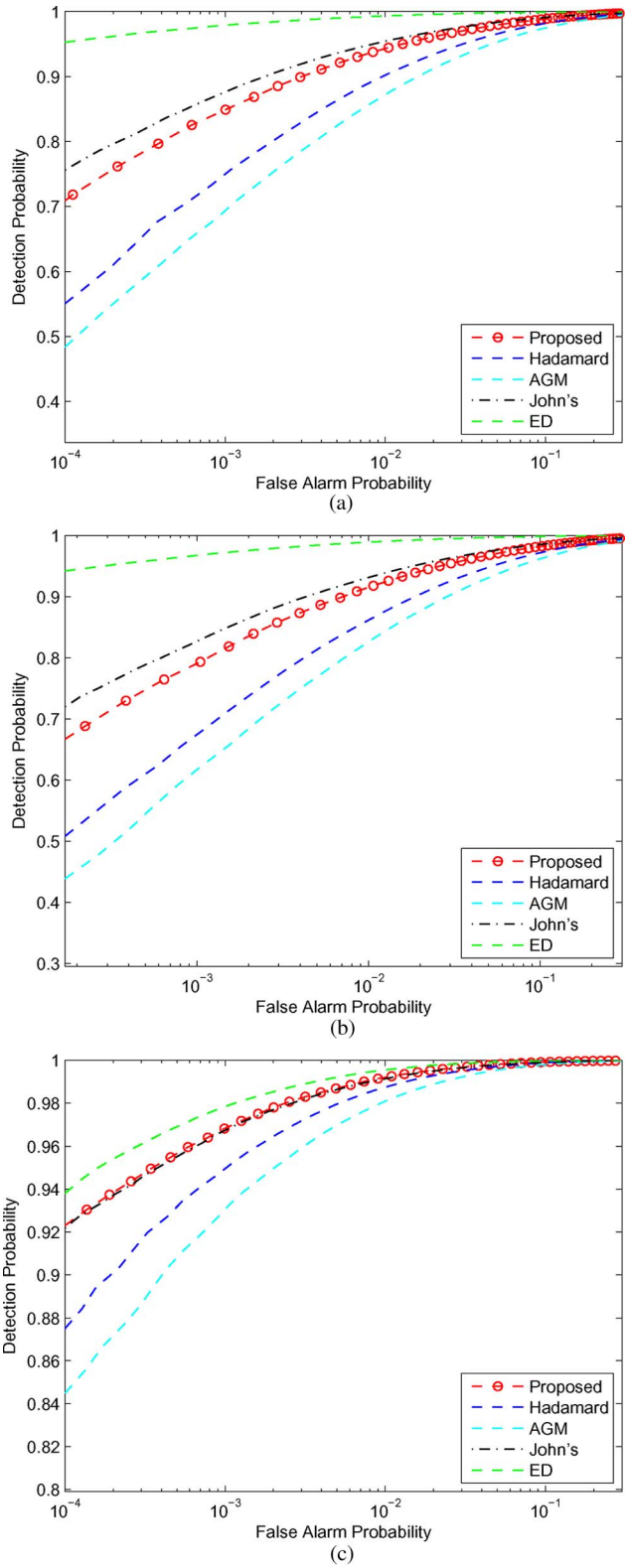

Fig. 6. ROCs of various detectors for Rayleigh fading channel in IID noise. (a) $M = 4$, $N = 10$, $d = 1$, and $\sigma_{s_1}^2 = 8$ dB. (b) $M = 4$, $N = 10$, $d = 3$, and $[\sigma_{s_1}^2, \sigma_{s_2}^2, \sigma_{s_3}^2] = [5, 2, 0]$ dB. (c) $M = 4$, $N = 50$, $d = 3$, and $[\sigma_{s_1}^2, \sigma_{s_2}^2, \sigma_{s_3}^2] = [0, -3, -5]$ dB.

Again, it is seen in Fig. 9 that the volume-based detector outperforms the robust Hadamard ratio test and non-robust AGM as well as John's approaches in detection accuracy. Moreover,

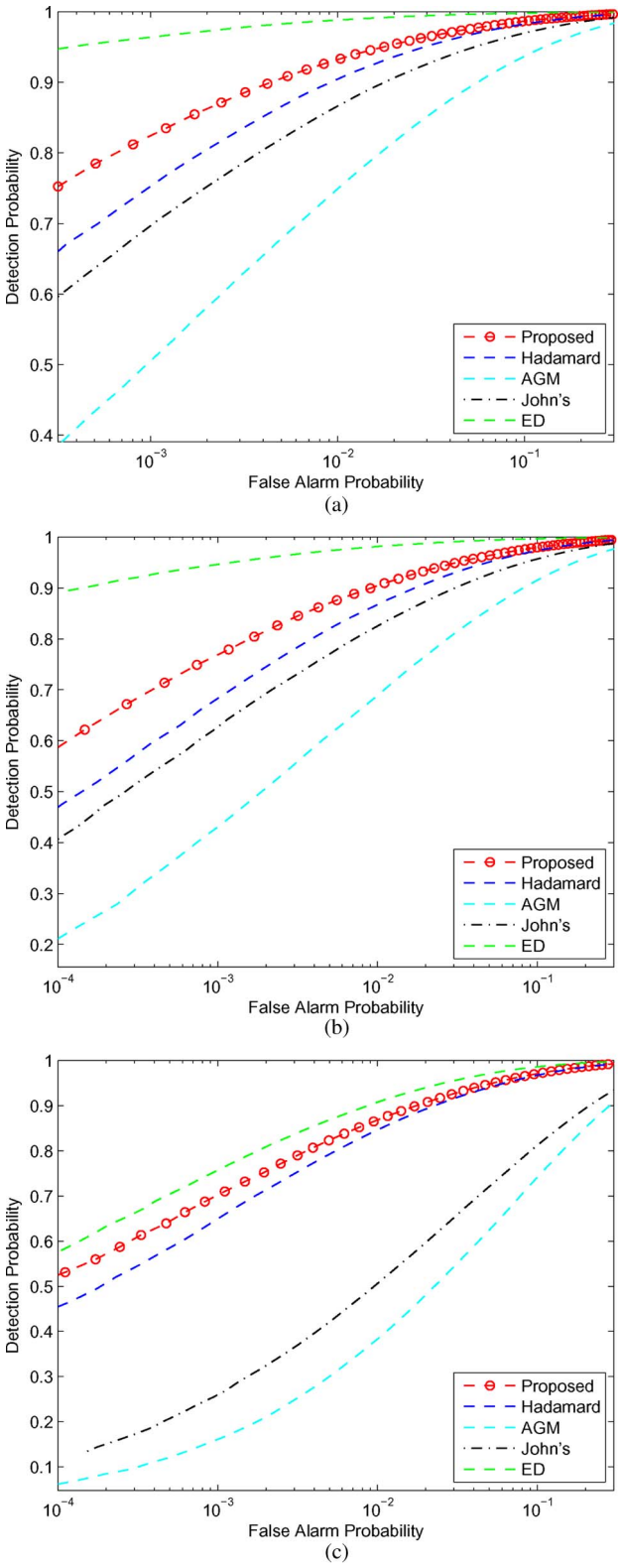

Fig. 7. ROCs of various detectors for Rayleigh fading channel in non-IID noise. (a) $M = 4$, $N = 10$, $d = 1$, and $\sigma^2_{s_1} = 8$ dB. (b) $M = 4$, $N = 10$, $d = 3$, and $[\sigma^2_{s_1}, \sigma^2_{s_2}, \sigma^2_{s_3}] = [5, 2, 0]$ dB. (c) $M = 4$, $N = 30$, $d = 3$, and $[\sigma^2_{s_1}, \sigma^2_{s_2}, \sigma^2_{s_3}] = [0, -3, -5]$ dB.

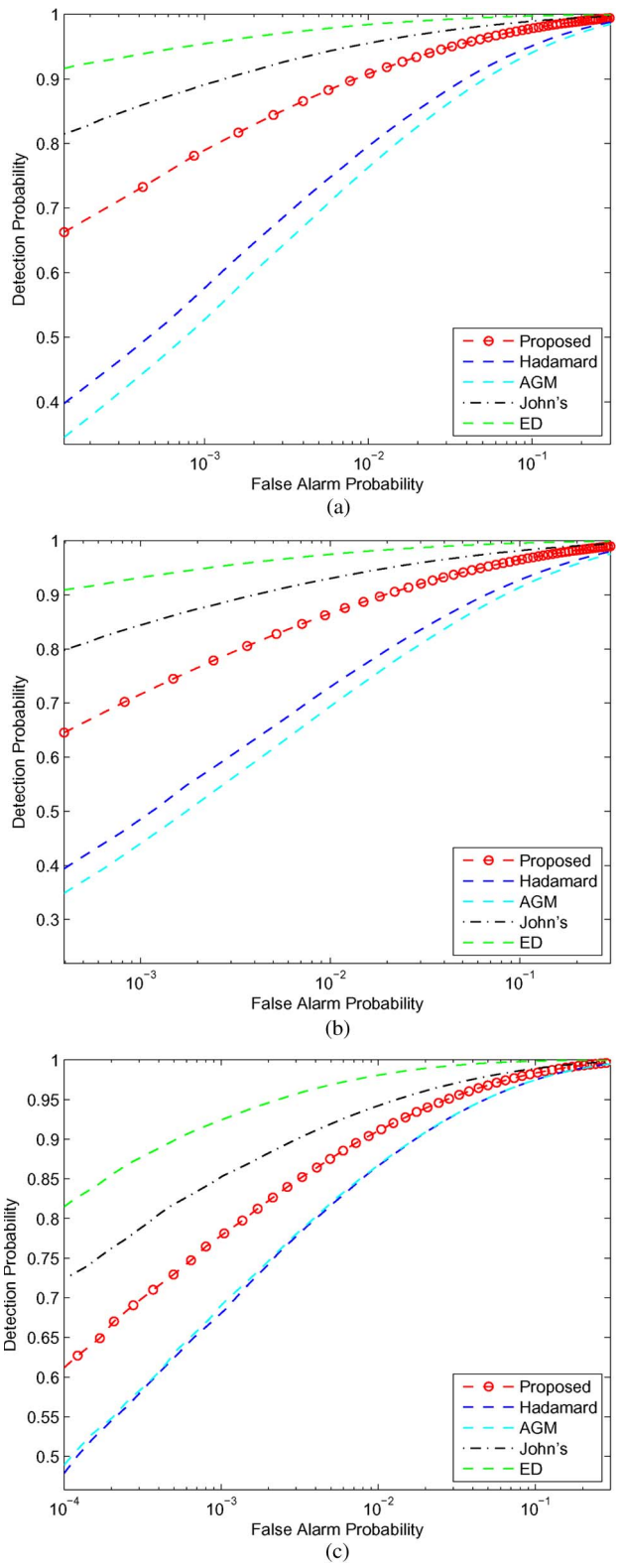

Fig. 8. ROCs of various detectors for Rayleigh fading channel in IID noise. (a) $M = 6$, $N = 10$, $d = 1$, and $\sigma^2_{s_1} = 8$ dB. (b) $M = 6$, $N = 10$, $d = 3$, and $[\sigma^2_{s_1}, \sigma^2_{s_2}, \sigma^2_{s_3}] = [5, 2, 0]$ dB. (c) $M = 6$, $N = 50$, $d = 3$, and $[\sigma^2_{s_1}, \sigma^2_{s_2}, \sigma^2_{s_3}] = [0, -3, -5]$ dB.

for $M = 6$, $N = 30$, and $[\sigma^2_{s_1}, \sigma^2_{s_2}, \sigma^3_{s_3}] = [0, -3, -5]$ dB, the volume-based algorithm is even superior to the ED scheme, as illustrated in Fig. 9(c).

V. Conclusion

The analytic formulae for the false-alarm and detection probabilities of the volume-based approach have been derived

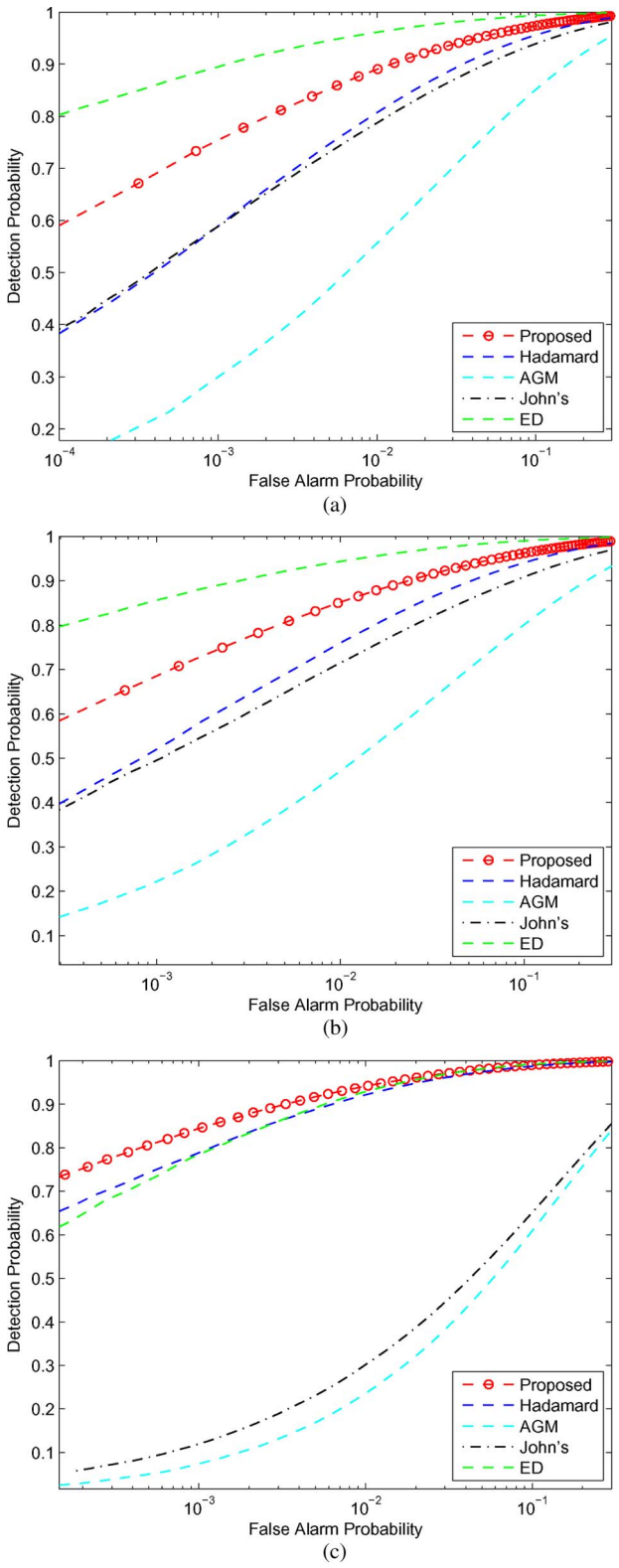

Fig. 9. ROCs of various detectors for Rayleigh fading channel in non-IID noise. (a) $M = 6$, $N = 10$, $d = 1$, and $\sigma_{s_1}^2 = 8$ dB. (b) $M = 6$, $N = 10$, $d = 3$, and $[\sigma_{s_1}^2, \sigma_{s_2}^2, \sigma_{s_3}^2] = [5, 2, 0]$ dB. (c) $M = 6$, $N = 50$, $d = 3$, and $[\sigma_{s_1}^2, \sigma_{s_2}^2, \sigma_{s_3}^2] = [0, -3, -5]$ dB.

for the IID noise, which provide accurate theoretical threshold calculation and efficient approach to evaluate its sensing performance. By means of calculating the accurate first and second moments of the test statistic under the signal-absence hypothesis, we are able to employ the moment-matching method to accurately derive the Gamma distribution. Accordingly, the theoretical decision threshold can be accurately determined as well. On the other hand, by computing the accurate first- and second-order moments of the test statistic under the signal-presence hypothesis, we are capable of approximating the Gamma distribution for the volume-based test statistic, ending up with accurate analytic expression for the detection probability. Extensive numerical results validate our theoretical analysis.

As has been pointed out in Sections I and IV-A, it is quite difficult to derive the false-alarm probability of the volume-based detector for the non-IID noise situations because the noise covariance matrix is unknown in practice. More specifically, the noise covariance matrix can be diagonal for non-uniform spatially white noise but arbitrary for spatially color noise. Derivation of the analytic false-alarm probability of the volume-based method in these non-IID noise scenarios will be our future work.

Appendix A
Proof of Proposition 1

Let $\boldsymbol{R} = N\boldsymbol{S} = \sum_{t=1}^{N} \boldsymbol{x}_t \boldsymbol{x}_t^{\mathrm{H}}$, which under $\mathcal{H}_1$ follows the complex Wishart distribution, i.e., $\boldsymbol{R} \sim \mathcal{W}_M(N, \boldsymbol{\Sigma})$. Setting $\varrho_k = \sum_{i=1}^{M} |r_{ki}|^2$ with r_{ki} being the (k, i) entry of $\boldsymbol{R}$, it follows from (12) that the volume-based test statistic becomes

$$\xi = \frac{1}{2}\sum_{k=1}^{M} \log \varrho_k - \log |\boldsymbol{R}|. \tag{A.1}$$

We utilize the Delta method to approximately calculate the first two moments of ξ. To proceed, we need to the following results of complex Bartlett decomposition thanks to Goodman [41].

Lemma 1: Let $\boldsymbol{R}' \sim \mathcal{W}_M(N, \boldsymbol{I}_M)$ and $\boldsymbol{R}' = \boldsymbol{T}\boldsymbol{T}^{\mathrm{H}}$ where $\boldsymbol{T} = (t_{ij})$ is a complex lower triangular matrix with real and positive diagonal elements, i.e., $t_{ii} > 0$, and non-diagonal elements $t_{ij} = t_{ij}^R + j t_{ij}^I$ $(j > i)$ with $_{ij}^R$ and $_{ij}^I$ being the real and imaginary parts of $_{ij}$, respectively. Then, the elements of $\boldsymbol{T}$ are all independent, $2t_{ii} \sim \chi^2_{2(N-i+1)}$ $(1 \le i \le M)$ with χ^2 being chi-square distribution and $t_{ij}^R \sim \mathcal{N}(0, 1/2)$, $t_{ij}^I \sim \mathcal{N}(0, 1/2)(1 \le j < i \le M)$.

According to Lemma 1, $\boldsymbol{R}$ can be represented in the form of $\boldsymbol{R} = \boldsymbol{A}\boldsymbol{T}\boldsymbol{T}^{\mathrm{H}}\boldsymbol{A}^{\mathrm{H}}$ with $\boldsymbol{A} = \boldsymbol{\Sigma}^{1/2}$. Then, the Taylor series expansion of

$$\xi \triangleq f(\boldsymbol{T}) = \frac{1}{2}\sum_{k=1}^{M} \log \varrho_k - 2\log |\boldsymbol{T}| - 2\log |\boldsymbol{A}| \tag{A.2}$$

in the neighborhood of the means of t_{ii}, t_{ij}^R and t_{ij}^I for $1 \le j < i \le M$ is given in (A.3), shown at the bottom of the next page. In the sequel, the second-order approximation to the mean of ξ, denoted as $\mu_1 \triangleq E[\xi]$, is

$$\mu_1 \approx f(\boldsymbol{T})|_{\boldsymbol{T}=E[\boldsymbol{T}]} + \frac{1}{2}\left[\sum_{j<i}^{M} \frac{\partial^2 f}{\partial \left(t_{ij}^R\right)^2}|_{\boldsymbol{T}=E[\boldsymbol{T}]} \mathrm{Var}\left(t_{ij}^R\right)\right.$$

$$+\sum_{j<i}^{M}\frac{\partial^2 f}{\partial\left(t_{ij}^{I}\right)^2}|_{\boldsymbol{T}=E[\boldsymbol{T}]}\mathrm{Var}\left(t_{ij}^{I}\right)+\sum_{i=1}^{M}\frac{\partial^2 f}{\partial\left(t_{ii}\right)^2}|_{\boldsymbol{T}=E[\boldsymbol{T}]}\mathrm{Var}\left(t_{ii}\right)\Bigg]. \quad \text{(A.4a)}$$

Additionally, the first-order approximation to the variance of ξ, denoted as $\nu_1 \triangleq \mathrm{Var}[\xi]$, is

$$\nu_1 \approx \sum_{j<i}^{M}\frac{\partial f}{\partial t_{ij}^{R}}\bigg|_{\boldsymbol{T}=E[\boldsymbol{T}]}\mathrm{Var}\left(t_{ij}^{R}\right)+\sum_{j<i}^{M}\frac{\partial f}{\partial t_{ij}^{I}}\bigg|_{\boldsymbol{T}=E[\boldsymbol{T}]}\mathrm{Var}\left(t_{ij}^{I}\right)+\sum_{i=1}^{M}\frac{\partial f}{\partial t_{ii}}\bigg|_{\boldsymbol{T}=E[\boldsymbol{T}]}\mathrm{Var}\left(t_{ii}\right). \quad \text{(A.4b)}$$

We are now at a position to determine the first two moments of the elements of $\boldsymbol{T}$, and the first and second-order partial derivatives of $f(\boldsymbol{T})$ with respect to the elements of $\boldsymbol{T}$. It follows from Lemma 1 that

$$E\left[t_{ij}^{R}\right]=E\left[t_{ij}^{I}\right]=0\,(1\le j<i\le M) \quad \text{(A.5a)}$$

$$\mathrm{Var}\left[t_{ij}^{R}\right]=\mathrm{Var}\left[t_{ij}^{I}\right]=\frac{1}{2}\,(1\le j<i\le M) \quad \text{(A.5b)}$$

$$E\left[t_{ii}\right]=\frac{\Gamma(n-i+\frac{3}{2})}{\Gamma(n-i+\frac{1}{2})}\,(1\le i\le M) \quad \text{(A.5c)}$$

$$\mathrm{Var}[t_{ii}]=n-i+1-\left(\frac{\Gamma(n-i+\frac{3}{2})}{\Gamma(n-i+\frac{1}{2})}\right)^2\,(1\le i\le M). \quad \text{(A.5d)}$$

On the other hand, the first-order partial derivatives of $f(\boldsymbol{T})$ with respect to t_{ij}^{R}, t_{ij}^{I}, and t_{ii} are computed in (A.6), shown at the bottom of the page. In addition, the second-order partial derivatives of $f(\boldsymbol{T})$ with respect to t_{ij}^{R}, t_{ij}^{I}, and t_{ii} are calculated by (A.7), shown at the bottom of the next page. Here, the first-order partial derivatives of r_{ij}^{R} and r_{ij}^{I} with respect to t_{ij}^{R}, t_{ij}^{I}, and t_{ii} are given, respectively, as

$$\frac{\partial r_{k\ell}^{R}}{\partial t_{ij}^{R}}=\left(a_{ik}^{R}a_{j\ell}^{R}+a_{ik}^{I}a_{j\ell}^{I}\right)E[t_{ii}] \quad \text{(A.8a)}$$

$$\frac{\partial r_{k\ell}^{R}}{\partial t_{ij}^{I}}=\left(a_{ik}^{I}a_{j\ell}^{R}-a_{ik}^{R}a_{j\ell}^{I}\right)E[t_{ii}] \quad \text{(A.8b)}$$

$$\begin{aligned}f(\boldsymbol{T})\approx f(\boldsymbol{T})|_{\boldsymbol{T}=E[\boldsymbol{T}]}&+\sum_{j<i}^{M}\frac{\partial f}{\partial t_{ij}^{R}}\bigg|_{\boldsymbol{T}=E[\boldsymbol{T}]}\left(t_{ij}^{R}-E\left[t_{ij}^{R}\right]\right)+\sum_{j<i}^{M}\frac{\partial f}{\partial t_{ij}^{I}}\bigg|_{\boldsymbol{T}=E[\boldsymbol{T}]}\left(t_{ij}^{I}-E\left[t_{ij}^{I}\right]\right)+\sum_{i=1}^{M}\frac{\partial f}{\partial t_{ij}}\bigg|_{\boldsymbol{T}=E[\boldsymbol{T}]}\left(t_{ij}-E\left[t_{ij}\right]\right)\\&+\frac{1}{2}\Bigg[\sum_{p<q}^{M}\sum_{j<i}^{M}\frac{\partial^2 f}{\partial t_{ij}^{R}\partial t_{pq}^{R}}\bigg|_{\boldsymbol{T}=E[\boldsymbol{T}]}\left(t_{ij}^{R}-E\left[t_{ij}^{R}\right]\right)\left(t_{pq}^{R}-E\left[t_{pq}^{R}\right]\right)+\sum_{p<q}^{M}\sum_{j<i}^{M}\frac{\partial^2 f}{\partial t_{ij}^{I}\partial t_{pq}^{I}}\bigg|_{\boldsymbol{T}=E[\boldsymbol{T}]}\left(t_{ij}^{I}-E\left[t_{ij}^{I}\right]\right)\left(t_{pq}^{I}-E\left[t_{pq}^{I}\right]\right)\\&+\sum_{p=1}^{M}\sum_{i=1}^{M}\frac{\partial^2 f}{\partial t_{pp}\partial t_{ii}}\bigg|_{\boldsymbol{T}=E[\boldsymbol{T}]}\left(t_{pp}-E\left[t_{pp}\right]\right)\left(t_{ii}-E\left[t_{ii}\right]\right)+2\sum_{p<q}^{M}\sum_{j<i}^{M}\frac{\partial^2 f}{\partial t_{ij}^{R}\partial t_{pq}^{I}}\bigg|_{\boldsymbol{T}=E[\boldsymbol{T}]}\left(t_{ij}^{R}-E\left[t_{ij}^{R}\right]\right)\left(t_{pq}^{I}-E\left[t_{pq}^{I}\right]\right)\\&+2\sum_{p=1}^{M}\sum_{j<i}^{M}\frac{\partial^2 f}{\partial t_{ij}^{R}\partial t_{pq}}\bigg|_{\boldsymbol{T}=E[\boldsymbol{T}]}\left(t_{ij}^{R}-E\left[t_{ij}^{R}\right]\right)\left(t_{pp}-E\left[t_{pp}\right]\right)+2\sum_{p=1}^{M}\sum_{j<i}^{M}\frac{\partial^2 f}{\partial t_{ij}^{I}\partial t_{pq}}\bigg|_{\boldsymbol{T}=E[\boldsymbol{T}]}\left(t_{ij}^{I}-E\left[t_{ij}^{I}\right]\right)\left(t_{pp}-E\left[t_{pp}\right]\right)\Bigg]\end{aligned} \quad \text{(A.3)}$$

$$\frac{\partial f}{\partial t_{ij}^{R}}\bigg|_{\boldsymbol{T}=E[\boldsymbol{T}]}=\frac{1}{2}\sum_{k=1}^{M}\sum_{\ell=1,k\neq\ell}^{M}\left[\frac{2r_{k\ell}^{R}}{\varrho_k}\frac{\partial r_{k\ell}^{R}}{\partial t_{ij}^{R}}+\frac{2r_{k\ell}^{I}}{\varrho_k}\frac{\partial r_{k\ell}^{I}}{\partial t_{ij}^{R}}\right]+\frac{1}{2}\sum_{k=1}^{M}\frac{2r_{kk}}{\varrho_k}\frac{\partial r_{kk}}{\partial t_{ij}^{R}} \quad \text{(A.6a)}$$

$$\frac{\partial f}{\partial t_{ij}^{I}}\bigg|_{\boldsymbol{T}=E[\boldsymbol{T}]}=\frac{1}{2}\sum_{k=1}^{M}\sum_{\ell=1,k\neq\ell}^{M}\left[\frac{2r_{k\ell}^{R}}{\varrho_k}\frac{\partial r_{k\ell}^{R}}{\partial t_{ij}^{I}}+\frac{2r_{k\ell}^{I}}{\varrho_k}\frac{\partial r_{k\ell}^{I}}{\partial t_{ij}^{I}}\right]+\frac{1}{2}\sum_{k=1}^{M}\frac{2r_{kk}}{\varrho_k}\frac{\partial r_{kk}}{\partial t_{ij}^{I}} \quad \text{(A.6b)}$$

$$\frac{\partial f}{\partial t_{ii}}\bigg|_{\boldsymbol{T}=E[\boldsymbol{T}]}=\frac{1}{2}\sum_{k=1}^{M}\sum_{\ell=1,k\neq\ell}^{M}\left[\frac{2r_{k\ell}^{R}}{\varrho_k}\frac{\partial r_{k\ell}^{R}}{\partial t_{ii}}+\frac{2r_{k\ell}^{I}}{\varrho_k}\frac{\partial r_{k\ell}^{I}}{\partial t_{ii}}\right]+\frac{1}{2}\sum_{k=1}^{M}\frac{2r_{kk}}{\varrho_k}\frac{\partial r_{kk}}{\partial t_{ii}}-\frac{2}{E[t_{ii}]} \quad \text{(A.6c)}$$

$$\frac{\partial r_{k\ell}^R}{\partial t_{ii}} = 2\left(a_{ik}^R a_{i\ell}^R + a_{ik}^I a_{i\ell}^I\right) E[t_{ii}] \tag{A.8c}$$

Moreover, the second-order partial derivatives of r_{ij}^R and r_{ij}^I with respect to t_{ij}^R, t_{ij}^I and t_{ii} are given, respectively, as

and

$$\frac{\partial r_{k\ell}^I}{\partial t_{ij}^R} = \left(a_{ik}^R a_{j\ell}^I - a_{ik}^I a_{j\ell}^R\right) E[t_{ii}] \tag{A.8d}$$

$$\frac{\partial r_{k\ell}^I}{\partial t_{ij}^I} = \left(a_{ik}^R a_{j\ell}^R + a_{ik}^I a_{j\ell}^I\right) E[t_{ii}] \tag{A.8e}$$

$$\frac{\partial r_{k\ell}^I}{\partial t_{ii}} = 2\left(a_{ik}^I a_{j\ell}^R - a_{ik}^R a_{j\ell}^I\right) E[t_{ii}]. \tag{A.8f}$$

$$\frac{\partial^2 r_{k\ell}^R}{\partial \left(t_{ij}^R\right)^2} = 2\left(a_{ik}^R a_{i\ell}^R + a_{ik}^I a_{i\ell}^I\right) \tag{A.8g}$$

$$\partial^2 r_{k\ell}^R \partial \left(t_{ij}^I\right)^2 = 2\left(a_{ik}^R a_{i\ell}^R + a_{ik}^I a_{i\ell}^I\right) \tag{A.8h}$$

$$\frac{\partial^2 r_{k\ell}^R}{\partial t_{ii}^2} = 2\left(a_{ik}^R a_{i\ell}^R - a_{ik}^I a_{i\ell}^I\right) \tag{A.8i}$$

$$\left.\frac{\partial^2 f}{\partial \left(t_{ij}^R\right)^2}\right|_{\boldsymbol{T}=E[\boldsymbol{T}]}$$
$$= \frac{1}{2}\sum_{k=1}^{M}\sum_{\ell=1,k\neq\ell}^{M}\left\{\sum_{p=1,p\neq k,p\neq\ell}^{M}\left[\frac{4r_{k\ell}^R r_{kp}^R}{\varrho_k^2}\frac{\partial r_{k\ell}^R}{\partial t_{ij}^R}\frac{\partial r_{kp}^R}{\partial t_{ij}^R} + \frac{4r_{k\ell}^R r_{kp}^I}{\varrho_k^2}\frac{\partial r_{k\ell}^R}{\partial t_{ij}^R}\frac{\partial r_{kp}^I}{\partial t_{ij}^R} + \frac{4r_{k\ell}^I r_{kp}^R}{\varrho_k^2}\frac{\partial r_{k\ell}^I}{\partial t_{ij}^R}\frac{\partial r_{kp}^R}{\partial t_{ij}^R} + \frac{4r_{k\ell}^I r_{kp}^I}{\varrho_k^2}\frac{\partial r_{k\ell}^I}{\partial t_{ij}^R}\frac{\partial r_{kp}^I}{\partial t_{ij}^R}\right]\right.$$
$$+ \frac{4r_{k\ell}^R r_{kk}}{\varrho_k^2}\frac{\partial r_{k\ell}^R}{\partial t_{ij}^R}\frac{\partial r_{kk}}{\partial t_{ij}^R} + \frac{4r_{k\ell}^I r_{kk}}{\varrho_k^2}\frac{\partial r_{k\ell}^I}{\partial t_{ij}^R}\frac{\partial r_{kk}}{\partial t_{ij}^R} + \frac{2\varrho_k - 4\left(r_{k\ell}^R\right)^2}{\varrho_k^2}\left(\frac{\partial r_{k\ell}^R}{\partial t_{ij}^R}\right)^2 + \frac{2r_{k\ell}^R}{\varrho_k}\frac{\partial^2 r_{k\ell}^R}{\partial \left(t_{ij}^R\right)^2}$$
$$\left. + \frac{2\varrho_k - 4\left(r_{k\ell}^I\right)^2}{\varrho_k^2}\left(\frac{\partial r_{k\ell}^I}{\partial t_{ij}^R}\right)^2 + \frac{2r_{k\ell}^I}{\varrho_k}\frac{\partial^2 r_{k\ell}^I}{\partial \left(t_{ij}^R\right)^2} + \frac{1}{2}\sum_{k=1}^{M}\left[\frac{2\varrho_k - 4r_{kk}^2}{\varrho_k^2}\left(\frac{\partial r_{kk}}{\partial t_{ij}^R}\right)^2 + \frac{2r_{kk}}{\varrho_k}\frac{\partial^2 r_{kk}}{\partial \left(t_{ij}^R\right)^2}\right]\right\} \tag{A.7a}$$

$$\left.\frac{\partial^2 f}{\partial \left(t_{ij}^I\right)^2}\right|_{\boldsymbol{T}=E[\boldsymbol{T}]}$$
$$= \frac{1}{2}\sum_{k=1}^{M}\sum_{\ell=1,k\neq\ell}^{M}\left\{\sum_{p=1,p\neq k,p\neq\ell}^{M}\left[\frac{4r_{k\ell}^R r_{kp}^R}{\varrho_k^2}\frac{\partial r_{k\ell}^R}{\partial t_{ij}^I}\frac{\partial r_{kp}^R}{\partial t_{ij}^I} + \frac{4r_{k\ell}^R r_{kp}^I}{\varrho_k^2}\frac{\partial r_{k\ell}^R}{\partial t_{ij}^I}\frac{\partial r_{kp}^I}{\partial t_{ij}^I} + \frac{4r_{k\ell}^I r_{kp}^R}{\varrho_k^2}\frac{\partial r_{k\ell}^I}{\partial t_{ij}^I}\frac{\partial r_{kp}^R}{\partial t_{ij}^I} + \frac{4r_{k\ell}^I r_{kp}^I}{\varrho_k^2}\frac{\partial r_{k\ell}^I}{\partial t_{ij}^I}\frac{\partial r_{kp}^I}{\partial t_{ij}^I}\right]\right.$$
$$+ \frac{4r_{k\ell}^R r_{kk}}{\varrho_k^2}\frac{\partial r_{k\ell}^R}{\partial t_{ij}^I}\frac{\partial r_{kk}}{\partial t_{ij}^I} + \frac{4r_{k\ell}^I r_{kk}}{\varrho_k^2}\frac{\partial r_{k\ell}^I}{\partial t_{ij}^I}\frac{\partial r_{kk}}{\partial t_{ij}^I} + \frac{2\varrho_k - 4\left(r_{k\ell}^R\right)^2}{\varrho_k^2}\left(\frac{\partial r_{k\ell}^R}{\partial t_{ij}^I}\right)^2 + \frac{2r_{k\ell}^R}{\varrho_k}\frac{\partial^2 r_{k\ell}^R}{\partial \left(t_{ij}^I\right)^2}$$
$$+ \frac{2\varrho_k - 4\left(r_{k\ell}^I\right)^2}{\varrho_k^2}\left(\frac{\partial r_{k\ell}^I}{\partial t_{ij}^I}\right)^2 + \frac{2r_{k\ell}^I}{\varrho_k}\frac{\partial^2 r_{k\ell}^I}{\partial \left(t_{ij}^I\right)^2}$$
$$\left. + \frac{1}{2}\sum_{k=1}^{M}\left[\frac{2\varrho_k - 4r_{kk}^2}{\varrho_k^2}\left(\frac{\partial r_{kk}}{\partial t_{ij}^I}\right)^2 + \frac{2r_{kk}}{\varrho_k}\partial^2 r_{kk}\partial\left(t_{ij}^I\right)^2\right]\right\} \tag{A.7b}$$

$$\left.\frac{\partial^2 f}{\partial t_{ii}^2}\right|_{\boldsymbol{T}=E[\boldsymbol{T}]}$$
$$= \frac{1}{2}\sum_{k=1}^{M}\sum_{\ell=1,k\neq\ell}^{M}\left\{\sum_{p=1,p\neq k,p\neq\ell}^{M}\left[\frac{4r_{k\ell}^R r_{kp}^R}{\varrho_k^2}\frac{\partial r_{k\ell}^R}{\partial t_{ii}}\frac{\partial r_{kp}^R}{\partial t_{ii}} + \frac{4r_{k\ell}^R r_{kp}^I}{\varrho_k^2}\frac{\partial r_{k\ell}^R}{\partial t_{ii}}\frac{\partial r_{kp}^I}{\partial t_{ii}} + \frac{4r_{k\ell}^I r_{kp}^R}{\varrho_k^2}\frac{\partial r_{k\ell}^I}{\partial t_{ii}}\partial r_{kp}^R\partial t_{ii} + \frac{4r_{k\ell}^I r_{kp}^I}{\varrho_k^2}\frac{\partial r_{k\ell}^I}{\partial t_{ii}}\frac{\partial r_{kp}^I}{\partial t_{ii}}\right]\right.$$
$$+ \frac{4r_{k\ell}^R r_{kk}}{\varrho_k^2}\frac{\partial r_{k\ell}^R}{\partial t_{ii}}\frac{\partial r_{kk}}{\partial t_{ii}} + \frac{4r_{k\ell}^I r_{kk}}{\varrho_k^2}\frac{\partial r_{k\ell}^I}{\partial t_{ii}}\frac{\partial r_{kk}}{\partial t_{ii}} + \frac{2\varrho_k - 4\left(r_{k\ell}^R\right)^2}{\varrho_k^2}\left(\frac{\partial r_{k\ell}^R}{\partial t_{ii}}\right)^2 + \frac{2r_{k\ell}^R}{\varrho_k}\partial^2 r_{k\ell}^R\partial t_{ii}^2$$
$$+ \frac{2\varrho_k - 4\left(r_{k\ell}^I\right)^2}{\varrho_k^2}\left(\frac{\partial r_{k\ell}^I}{\partial t_{ii}}\right)^2 + \frac{2r_{k\ell}^I}{\varrho_k}\frac{\partial^2 r_{k\ell}^I}{\partial t_{ii}^2}$$
$$\left. + \frac{1}{2}\sum_{k=1}^{M}\left[\frac{2\varrho_k - 4r_{kk}^2}{\varrho_k^2}\left(\frac{\partial r_{kk}}{\partial t_{ii}}\right)^2 + \frac{2r_{kk}}{\varrho_k}\frac{\partial^2 r_{kk}}{\partial t_{ii}^2}\right]\right\} + \frac{2}{E^2[t_{ii}]} \tag{A.7c}$$

and

$$\frac{\partial^2 r_{k\ell}^I}{\partial \left(t_{ij}^R\right)^2} = 2\left(a_{jk}^I a_{j\ell}^R - a_{jk}^R a_{j\ell}^I\right) \tag{A.8j}$$

$$\frac{\partial^2 r_{k\ell}^I}{\partial \left(t_{ij}^I\right)^2} = 2\left(a_{jk}^I a_{j\ell}^R - a_{jk}^R a_{j\ell}^I\right) \tag{A.8k}$$

$$\frac{\partial^2 r_{k\ell}^I}{\partial t_{ii}^2} = 2\left(a_{ik}^I a_{i\ell}^R - a_{ik}^R a_{j\ell}^I\right). \tag{A.8l}$$

Furthermore, we easily obtain

$$\frac{\partial r_{kk}}{\partial t_{ij}^R} = \left(a_{ik}^R a_{jk}^R + a_{ik}^I a_{jk}^I\right) E[t_{ii}] \tag{A.8m}$$

$$\frac{\partial r_{kk}}{\partial t_{ij}^I} = \left(a_{ik}^I a_{jk}^R - a_{ik}^R a_{jk}^I\right) E[t_{ii}] \tag{A.8n}$$

$$\frac{\partial r_{kk}}{\partial t_{ii}} = 2\left(\left(a_{ik}^R\right)^2 + \left(a_{ik}^I\right)^2\right) E[t_{ii}] \tag{A.8o}$$

and

$$\frac{\partial^2 r_{kk}}{\partial \left(t_{ij}^R\right)^2} = 2\left(\left(a_{jk}^R\right)^2 + \left(a_{jk}^I\right)^2\right) \tag{A.8p}$$

$$\frac{\partial^2 r_{kk}}{\partial \left(t_{ij}^I\right)^2} = 2\left(\left(a_{jk}^R\right)^2 + \left(a_{jk}^I\right)^2\right) \tag{A.8q}$$

$$\frac{\partial^2 r_{kk}}{\partial t_{ii}^2} = 2\left(\left(a_{ik}^R\right)^2 + \left(a_{ik}^I\right)^2\right). \tag{A.8r}$$

Substituting (A.8) into (A.6) and (A.7), and then inserting the so-obtained results along with (A.5) into (A.4), we eventually attain the mean μ_1 and variance ν_1 for calculating α_1 and β_1 in (14). This completes the proof of Proposition 1.

Appendix B
Proof of Proposition 2

For the signal-absence hypothesis, we have $\boldsymbol{A} = \boldsymbol{I}_M$. It follows from (A.4) and (A.5) that the mean and variance of ξ under $\mathcal{H}_0$, denoted by μ_0 and ν_0, respectively, can be given as

$$\mu_0 \approx f(\boldsymbol{T})|_{\boldsymbol{T}=E[\boldsymbol{T}]} + \frac{1}{4}\sum_{j<i}^{M}\left(\frac{\partial^2 f}{\partial\left(t_{ij}^R\right)^2} + \frac{\partial^2 f}{\partial\left(t_{ij}^I\right)^2}\right)\Bigg|_{\boldsymbol{T}=E[\boldsymbol{T}]} + \frac{1}{2}\sum_{i=1}^{M}\left(n-i+1-\left(\frac{\Gamma(n-i+\frac{3}{2})}{\Gamma(n-i+\frac{1}{2})}\right)^2\right)\frac{\partial^2 f}{\partial\left(t_{ii}\right)^2}\Bigg|_{\boldsymbol{T}=E[\boldsymbol{T}]} \tag{B.1a}$$

and

$$\nu_0 \approx \frac{1}{2}\sum_{j<i}^{M}\left(\frac{\partial f}{\partial t_{ij}^R} + \frac{\partial f}{\partial t_{ij}^I}\right)\Bigg|_{\boldsymbol{T}=E[\boldsymbol{T}]} + \sum_{i=1}^{M}\left(n-i+1-\left(\frac{\Gamma(n-i+\frac{3}{2})}{\Gamma(n-i+\frac{1}{2})}\right)^2\right)\frac{\partial f}{\partial t_{ii}}\Bigg|_{\boldsymbol{T}=E[\boldsymbol{T}]}. \tag{B.1b}$$

where $f(\boldsymbol{T}) = (1/2)\sum_{k=1}^{M}\log\varrho_k - 2\log|\boldsymbol{T}|$. Moreover, it follows from (A.6), (A.7), and (A.8) that the first and second-order partial derivatives of $f(\boldsymbol{T})$ with respect to the elements of $\boldsymbol{T}$ can be simplified, respectively, as

$$\frac{\partial f}{\partial t_{ij}^R}\Bigg|_{\boldsymbol{T}=E[\boldsymbol{T}]} = \left(\frac{r_{ij}^R}{\varrho_j} + \frac{r_{ij}^R}{\varrho_i}\right)\frac{\partial r_{ij}^R}{\partial t_{ij}^R} \tag{B.2a}$$

$$\frac{\partial f}{\partial t_{ij}^I}\Bigg|_{\boldsymbol{T}=E[\boldsymbol{T}]} = \left(\frac{r_{ij}^I}{\varrho_j} + \frac{r_{ij}^I}{\varrho_i}\right)\frac{\partial r_{ij}^I}{\partial t_{ij}^I} \tag{B.2b}$$

$$\frac{\partial f}{\partial t_{ii}}\Bigg|_{\boldsymbol{T}=E[\boldsymbol{T}]} = \frac{r_{ii}}{\varrho_i}\frac{\partial r_{ii}}{\partial t_{ii}} - \frac{2}{E[t_{ii}]} \tag{B.2c}$$

and

$$\frac{\partial^2 f}{\partial\left(t_{ij}^R\right)^2}\Bigg|_{\boldsymbol{T}=E[\boldsymbol{T}]} = \left(\frac{\varrho_j - 2\left(r_{ij}^R\right)^2}{\varrho_j^2} + \frac{\varrho_i - 2\left(r_{ij}^R\right)^2}{\varrho_i^2}\right)\left(\frac{\partial r_{ij}^R}{\partial t_{ij}^R}\right)^2 + \frac{r_{jj}}{\varrho_j}\frac{\partial^2 r_{jj}}{\partial\left(t_{ij}^R\right)^2} \tag{B.3a}$$

$$\frac{\partial^2 f}{\partial\left(t_{ij}^I\right)^2}\Bigg|_{\boldsymbol{T}=E[\boldsymbol{T}]} = \left(\frac{\varrho_j - 2\left(r_{ij}^I\right)^2}{\varrho_j^2} + \frac{\varrho_i - 2\left(r_{ij}^I\right)^2}{\varrho_i^2}\right)\left(\frac{\partial r_{ij}^I}{\partial t_{ij}^I}\right)^2 + \frac{r_{jj}}{\varrho_j}\frac{\partial^2 r_{jj}}{\partial\left(t_{ij}^I\right)^2} \tag{B.3b}$$

$$\frac{\partial^2 f}{\partial\left(t_{ii}\right)^2}\Bigg|_{\boldsymbol{T}=E[\boldsymbol{T}]} = \frac{\varrho_i - 2r_{ii}^2}{\varrho_i^2}\left(\frac{\partial r_{ii}}{\partial t_{ii}}\right)^2 + \frac{r_{ii}}{\varrho_i}\frac{\partial^2 r_{ii}}{\partial\left(t_{ii}\right)^2} + \frac{2}{E^2[t_{ii}]} \tag{B.3c}$$

where

$$\frac{\partial r_{ii}}{\partial t_{ii}} = 2\frac{\partial r_{ij}^R}{\partial t_{ij}^R} = 2\frac{\partial r_{ij}^I}{\partial t_{ij}^I} = 2E[t_{ii}] \tag{B.4a}$$

$$\frac{\partial^2 r_{jj}}{\partial\left(t_{ij}^R\right)^2} = \frac{\partial^2 r_{jj}}{\partial\left(t_{ij}^I\right)^2} = \frac{\partial^2 r_{ii}}{\partial\left(t_{ii}\right)^2} = 2. \tag{B.4b}$$

Thus, inserting (B.4) into (B.2) and (B.3), and then substituting the so-obtained results into (B.1) yield μ_0 and ν_0 for computing α_0 and β_0 in (17). The proof of Proposition 2 is finished.

References

[1] J. Mitola, III, "Cognitive radio for flexible mobile multimedia communications," in *Proc. IEEE Int. Workshop MoMuC*, San Diego, CA, USA, Nov. 1999, pp. 3–10.

[2] S. Haykin, "Cognitive radio: Brain-empowered wireless communications," *IEEE J. Sel. Areas Commun.*, vol. 23, no. 2, pp. 201–220, Feb. 2005.

[3] P. Wang, J. Fang, N. Han, and H. Li, "Multiantenna-assisted spectrum sensing for cognitive radio," *IEEE Trans. Veh. Technol.*, vol. 59, no. 4, pp. 1791–1800, May 2010.

[4] A. Taherpour, M. Nasiri-Kenari, and S. Gazor, "Multiple antenna spectrum sensing in cognitive radios," *IEEE Trans. Wireless Commun.*, vol. 9, no. 2, pp. 814–823, Nov. 2010.

[5] H. Urkowitz, "Energy detection of unknown deterministic signals," *Proc. IEEE*, vol. 55, no. 4, pp. 523–531, Apr. 1967.

[6] F. F. Digham, M. S. Alouini, and M. K. Simon, "On the energy detection of unknown signals over fading channels," *IEEE Trans. Commun.*, vol. 55, no. 1, pp. 21–24, Jan. 2007.
[7] A. Mariani, A. Giorgetti, and M. Chiani, "Effects of noise power estimation on energy detection for cognitive radio applications," *IEEE Trans. Comput.*, vol. 59, no. 12, pp. 3410–3420, Dec. 2011.
[8] V. Koivunen, S. Chaudhari, and H. V. Poor, "Autocorrelation-based decentralized sequential detection of OFDM signals in cognitive radios," *IEEE Trans. Signal Process.*, vol. 57, no. 7, pp. 2690–2700, Jul. 2009.
[9] A. Huttunen, J. Lundén, V. Koivunen, and H. V. Poor, "Spectrum sensing in cognitive radios based on multiple cyclic frequencies," in *Proc. 2nd Int. Conf. Cognitive Radio Oriented Wireless Netw. Commun.*, Orlando, FL, USA, Aug. 2007, pp. 37–43.
[10] A. Huttunen, J. Lundén, V. Koivunen, and H. V. Poor, "Collaborative cyclostationary spectrum sensing for cognitive radio systems," *IEEE Trans. Signal Process.*, vol. 57, no. 11, pp. 4182–4195, Nov. 2009.
[11] Z. Tian, Y. Tafesse, and B. M. Sadler, "Cyclic feature detectionwith sub-Nyquist sampling for wideband spectrum sensing," *IEEE J. Sel. Topics Signal Process.*, vol. 6, no. 1, pp. 58–69, Feb. 2012.
[12] Y. Zeng, C. L. Koh, and Y.-C. Liang, "Maximum eigenvalue detection: Theory and application," in *Proc. IEEE ICC*, Beijing, China, May 2008, pp. 4160–4164.
[13] A. Kortun, T. Ratnarajah, M. Sellathurai, C. Zhong, and C. B. Papadias, "On the performance of eigenvalue-based cooperative spectrum sensing for cognitive radio," *IEEE J. Sel. Topics Signal Process.*, vol. 5, no. 1, pp. 49–55, Feb. 2011.
[14] Q. T. Zhang, "Theoretical performance and thresholds of the multitaper method for spectrum sensing," *IEEE Trans. Veh. Technol.*, vol. 60, no. 5, pp. 2128–2138, Jun. 2011.
[15] L. Wei, P. Dharmawansa, and O. Tirkkonen, "Multiple primary user spectrum sensing in the low SNR regime," *IEEE Trans. Commun.*, vol. 61, no. 5, pp. 1720–1731, May 2013.
[16] L. Wei and O. Tirkkonen, "Spectrum sensing in the presence of multiple primary users," *IEEE Trans. Commun.*, vol. 60, no. 5, pp. 1268–1277, May 2012.
[17] R. Zhang, T. Lim, Y.-C. Liang, and Y. Zeng, "Multi-antenna based spectrum sensing for cognitive radios: A GLRT approach," *IEEE Trans. Commun.*, vol. 58, no. 1, pp. 84–88, Jan. 2010.
[18] T. J. Lim, R. Zhang, Y. C. Liang, and Y. H. Zeng, "GLRT-based spectrum sensing for cognitive radio," in *Proc. IEEE GLOBECOM*, New Orleans, LA, USA, Dec. 2008, pp. 1–5.
[19] O. Ledoit and M. Wolf, "Some hypothesis tests for the covariance matrix when the dimension is large compared to the sample size," *Ann. Statist.*, vol. 30, no. 4, pp. 1081–1102, 2002.
[20] S. John, "Some optimal multivariate tests," *Biometrika*, vol. 58, no. 1, pp. 123–127, Apr. 1971.
[21] A. Gokceoglu, S. Dikmese, M. Valkama, and M. Renfors, "Energy detection under IQ imbalance with single- and multi-channel direct-conversion receiver: Analysis and mitigation," *IEEE J. Sel. Areas Commun.*, vol. 32, no. 3, pp. 411–424, Mar. 2014.
[22] A. Gokceoglu, S. Dikmese, M. Valkama, and M. Renfors, "Analysis and mitigation of RF IQ imbalance in eigenvalue based multichannel spectrum sensing," in *Proc. 24th Int. Symp. PIMRC*, London, U.K., Sep. 2013, pp. 734–739.
[23] J. K. Tugnait, "On multiple antenna spectrum sensing under noise variance uncertainty and flat fading," *IEEE Trans. Signal Process.*, vol. 60, no. 4, pp. 1823–1832, Apr. 2012.
[24] A. Mariani, A. Giorgetti, and M. Chiani, "Test of independence for cooperative spectrum sensing with uncalibrated receivers," in *Proc. IEEE GLOBECOM*, Anaheim, CA, USA, Dec. 2012, pp. 1374–1379.
[25] D. Ramírez, G. Vazquez-Vilar, R. López-Valcarce, J. Vía, and I. Santamaría, "Detection of rank-p signals in cognitive radio networks with uncalibrated multiple antennas," *IEEE Trans. Signal Process.*, vol. 59, no. 8, pp. 3764–3774, Aug. 2011.
[26] R. López-Valcarce, G. Vazquez-Vilar, and J. Sala, "Multiantenna spectrum sensing for cognitive radio: Overcoming noise uncertainty," in *Proc. 2nd Int. Workshop CIP*, Elba, Italy, Jun. 2010, pp. 310–315.
[27] R. Li, L. Huang, Y. Shi, and H. C. So, "Gerschgorin disk-based robust spectrum sensing for cognitive radio," in *Proc. IEEE ICASSP*, Florence, Italy, May 2014, pp. 1–4.
[28] J. Vía, D. Ramírez, and I. Santamaría, "The locally most powerful test for multiantenna spectrum sensing with uncalibrated receivers," in *Proc. IEEE ICASSP*, Kyoto, Japan, Mar. 2012, pp. 3437–3440.
[29] L. Huang, H. C. So, and C. Qiang, "Volume-based method for spectrum sensing," *Digit. Signal Process.*, vol. 28, pp. 1–9, May 2014.
[30] S. Wilks, "On the independence of k sets of normally distributed statistical variables," *Econometrica*, vol. 3, no. 3, pp. 309–325, Jul. 1935.
[31] A. Leshem and A.-J. van der Veen, "Multichannel detection of Gaussian signals with uncalibrated receivers," *IEEE Signal Process. Lett.*, vol. 8, no. 4, pp. 120–122, Apr. 2001.
[32] A. Leshem and A.-J. van der Veen, "Multichannel detection and spatial signature estimation with uncalibrated receivers," in *Proc. 11th IEEE Workshop Statist. Signal Process.*, Singapore, Dec. 2001, pp. 190–193.
[33] G. H. Golub and C. F. V. Loan, *Matrix Computation: 3rd Edition*. Baltimore, MD, USA: The Johns Hopkins Univ. Press, 1995.
[34] L. Huang, T. Long, and S. Wu, "Source enumeration for high-resolution array processing using improved Gerschgorin radii without eigendecomposition," *IEEE Trans. Signal Process.*, vol. 56, no. 12, pp. 5916–5925, Dec. 2008.
[35] S. Dikmese *et al.*, "Reducing computational complexity of eigenvalue based spectrum sensing for cognitive radio," in *Proc. 8th Int. Conf. CROWNCOM*, Washington, DC, USA, Jul. 2013, pp. 61–67.
[36] S. Dikmese, A. Gokceoglu, M. Valkama, and M. Renfors, "Reduced complexity spectrum sensing based on maximum eigenvalue and energy," in *Proc. 10th ISWCS*, Ilmenau, Germany, Aug. 2013, pp. 1–5.
[37] A. Abdi, J. A. Barger, and M. Kaveh, "A parametric model for the distribution of the angle of arrival and the associated correlation function and power spectrum at the mobile station," *IEEE Trans. Veh. Technol.*, vol. 53, no. 3, pp. 425–434, May 2002.
[38] A. Abdi and M. Kaveh, "A space-time correlation model for multielement antenna systems in mobile fading channels," *IEEE J. Select. Areas Commun.*, vol. 20, no. 3, pp. 550–560, Apr. 2002.
[39] Y. R. Zheng and C. Xiao, "Simulation models with correct statistical properties for Rayleigh fading channels," *IEEE Trans. Comput.*, vol. 51, no. 6, pp. 920–928, Jun. 2003.
[40] M. Chiani, M. Z. Win, and A. Zanella, "On the capacity of spatially correlated MIMO Rayleigh-fading channels," *IEEE Trans. Inf. Theory*, vol. 49, no. 10, pp. 2363–2371, Oct. 2003.
[41] N. R. Goodman, "Statistical analysis based on a certain multivariate complex Gaussian distribution (an introduction)," *Annals Math. Stat.*, vol. 34, no. 1, pp. 152–177, Mar. 1963.

Lei Huang (M'07) was born in Guangdong, China. He received the B.Sc., M.Sc., and Ph.D. degrees in electronic engineering from Xidian University, Xi'an, China, in 2000, 2003, and 2005, respectively.

From 2005 to 2006, he was a Research Associate with the Department of Electrical and Computer Engineering, Duke University, Durham, NC. From 2009 to 2010, he was a Research Fellow with the Department of Electronic Engineering, City University of Hong Kong and a Research Associate with the Department of Electronic Engineering, The Chinese University of Hong Kong. Since 2011, he has joined the Department of Electronic and Information Engineering, Harbin Institute of Technology Shenzhen Graduate School, where he is currently a Professor. His research interests include spectral estimation, array signal processing, statistical signal processing, and their applications in radar and wireless communication systems.

He currently is an editorial board member of Digital Signal Processing.

Cheng Qian was born in Zhejiang on November 27, 1988. He received the B.E. degree in communication engineering from Hangzhou Dianzi University, Hangzhou, China, in 2011, and M.E. degree in information and communication engineering from Harbin Institute of Technology (HIT), Shenzhen, China, in 2013. He is currently pursuing the Ph.D. degree in the field of information and communication engineering at HIT. His research interests are in array signal processing and MIMO radar.

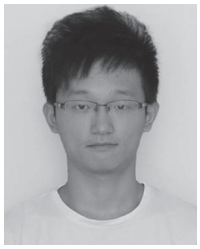

Yuhang Xiao was born in Anhui on January 20, 1992. He received the B.E. degree from Harbin Engineering University, Harbin, China, in 2012. He is currently pursuing the Ph.D. degree in the field of communication and information engineering at HIT. His research interests are in statistical signal processing and spectrum sensing.

Q. T. Zhang (S'84–M'85–SM'95–F'09) received the B.Eng. degree from Tsinghua University, Beijing, China and M.Eng. degree from South China University of Technology, Guangzhou, China, both in wireless communications, and the Ph.D. degree in electrical engineering from McMaster University, Hamilton, ON, Canada.

After graduation from McMaster in 1986, he held a research position and Adjunct Assistant Professorship at the same institution. In January 1992, he joined the Spar Aerospace Ltd., Satellite and Communication Systems Division, Montreal, as a Senior Member of Technical Staff. At Spar Aerospace, he participated in the development and manufacturing of the Radar Satellite (Radarsat). He joined Ryerson University, Toronto in 1993 and became a Professor in 1999. In 1999, he took one-year sabbatical leave at the National University of Singapore, and was a Chair Professor of Information Engineering at the City University of Hong Kong. His research interest is on wireless communications with current focus on wireless MIMO, cooperative systems, and cognitive radio. He served as an Associate Editor for the IEEE Communications Letters from 2000 to 2007.